Int. J. Econ. Environ. Geol. Vol. 16 (3) 66-78, 2025
Journal home page: www.econ-environ-geol.org

Open Access
ISSN (Online) 2223-957X

Biotite Chemistry from the Chah-Firozeh Deposit, Kerman Cenozoic Magmatic Arc, Iran: Implication for Porphyry Copper Mineralization

Johar Ali*, Sina Asadi, Arezou Alsadat Mirbagheri Dehaghani

University, Shiraz, Iran Department of Earth Sciences, School of Science, Shiraz, Iran

Corresponding author E-mail: joharaliirfani@gmail.com

Received: *11 August, 2025* ***Accepted:*** *27 September, 2025*

Abstract: The Chah-Firozeh porphyry Cu system is situated within Kerman Cenozoic Magmatic Arc (KCMA), was examined using integrated petrographic observations and quantitative electron probe microanalysis (EPMA) EPMA analyses to elucidate its magmatic–hydrothermal evolution and metallogenic characteristics. The deposit is hosted by Eocene andesitic volcanic sequences and is intruded by a Miocene porphyritic stock ranging in composition from quartz monzodiorite to quartz diorite. Hydrothermal alteration is well developed and consists of potassic, phylitic, and propylitic zones, locally overprinted by silicic and late supergene argillic assemblages. Ore mineralization is predominantly hosted in quartz–sulfide veins, stockwork networks, and as disseminated grains of chalcopyrite, bornite, molybdenite, and pyrite. Biotite, a widespread ferromagnesian phase in both magmatic and hydrothermal domains, was analyzed to constrain physicochemical parameters of fluid evolution. Distinct compositional trends in major elements, halogens, and Fe/Mg ratios delineate multiple magmatic and hydrothermal fluid pulses, reflecting changes in temperature, oxidation state, and halogen fugacity. Halogen contents and calculated fugacity ratios (fCl/fH_2O, fF/fH_2O) provide an effective geochemical discriminator between barren and mineralized intrusions across the KCMA. These findings confirm that biotite is a reliable porphyry indicator mineral (PIM) and a sensitive tracer of petrogenetic and metallogenic processes in Andean-type arc settings.

Keywords: Chah-Firozeh, Kerman Cenozoic Magmatic Arc, Porphyry deposit, Biotite chemistry, Halogen fugacity.

Introduction

Biotite, a trioctahedral mica containing halogens, is a key mineral for investigating the formation and hydrothermal development of porphyry Cu ± Mo ± Au deposits. The ferromagnesian phase, ubiquitous in both magmatic and hydrothermal systems, exhibits chemical compositions that are highly sensitive to intensive variables, including temperature, oxygen fugacity, water activity, and halogen fugacity (Wones and Eugster, 1965; Speer, 1987; Tang et al., 2019).

High-precision techniques such as EPMA enable accurate quantification of major, minor, and halogen elements in biotite, enhancing its role as a porphyry indicator mineral (PIM). Magmatic and hydrothermal biotites from the Chah-Firozeh porphyry copper deposit, within the Kerman Cenozoic Magmatic Arc (KCMA), are examined in this study. Through systematic microchemical characterization, we aim to: (1) delineate compositional differences between magmatic and hydrothermal biotites; (2) constrain physicochemical parameters (temperature, fO_2, fH_2O, fugacity halogen) prevailing during different stages of ore-forming processes; and (3) assess the potential of halogen-bearing biotite as a robust exploration tool in Cu–Mo–Au porphyry systems.

While the compositional variability of biotite in both magmatic and hydrothermal settings has been extensively reported (Beane, 1974; Afshooni et al., 2013; Tang et al., 2019), only a limited number of studies have focused on biotite formed specifically under hydrothermal alteration conditions (Yang, 1964; Tang et al., 2016). This study provides a detailed, high-resolution geochemical dataset that sheds light on biotite evolution in porphyry-style mineralization and refines biotite-based exploration guidelines for the KCMA and similar arc-related metallogenic belts.

Geological Setting

The Chah-Firozeh porphyry Cu deposit occurs in the Kerman segment of the Urumiyeh–Dokhtar Magmatic Belt, southern Iran. As a major eastern

Tethyan metallogenic belt, the UDMB reflects magmatic and metallogenic evolution driven by Neo-Tethyan subduction and later Arabian–Eurasian collision (Alavi, 1980; Berberian, 1982; Asadi et al., 2015).

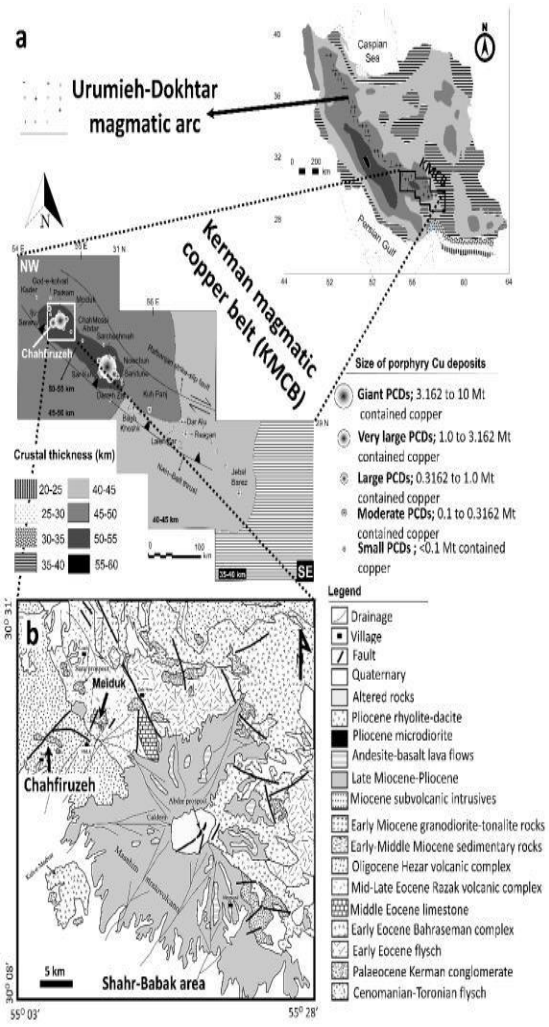

Fig. 1 (a) Schematic illustration of Moho depth (grey shading) and crustal thickness (km) across the Kerman Magmatic– Copper Belt (KMCB), highlighting two geodynamically distinct segments extending from the northwestern Kuh- Panj–type domain to the southeastern Jebal-Barez–type domain. The spatial distribution and relative sizes of porphyry Cu deposits andprospects within the Meiduk cluster are shown (after Saric & Mijalkovic, 1973). Inset map illustrates present-day crustal thickness variations across Iran, compiled and simplified after Dehghani & Makris (1983), and modified following Shafiei et al. (2009).(b) Regional geological map of the Shahr- Babak area in the northwestern KMCB, showing the location of the Chah-Firuzeh porphyry Cu system (CFP), situated ~15 km SW southwest of the Meiduk deposit (modified after Taghipour et al., 2008). **Abbreviations:** KDP: Keder prospect, IJP: Iju porphyry, GKP: God–e–Kolvary prospect, SNP: Serenu prospect, CFP: Chah Firuzeh porphyry, PAP: Parkam (Sara) porphyry, MP: Meiduk porphyry, ABP: Abdar porphyry, CMP: Chah Messi porphyry, SKP: Sar Kuh porphyry, NP: Now Chon porphyry, SCP: Sarcheshmeh porphyry, DZP: Darreh Zar porphyry, SDP: Saridune prospect, KPP: Kuh Panj porphyry, BKP: Bagh Khoshk Sharghi porphyry, LZP: Lalleh Zar prospect, DAP: Dar Alu porphyry, REP: Reagan porphyry, JBP: Jebal Barez porphyry.

The study area is confined between the Sanandaj–Sirjan belt and the Central Iranian blocks, with porphyry mineralization linked to terminal Neo-Tethyan closure and Miocene Arabian–Iranian collision. The Kerman Cenozoic Magmatic Arc (KCMA) exhibits a NNW–SSE structural trend, extending ~450 km, and is 60–80 km western side of Central Iranian block (Zarasvandi et al., 2018). The belt occurs more than 20 porphyry copper deposits and prospects, which are conventionally classified into two main categories: (i) younger, economically viable porphyry systems (e.g., Kuh-e-Panj), and (ii) older porphyry occurrences that are sub-economic to barren (Jebal-e-Barez) (Asadi et al., 2014).

The Chah-Firozeh deposit is widely interpreted as an economically significant porphyry copper system associated with late-stage mineralizing events; however, alternative assessments have characterized it as sub-economic based on resource potential and grade considerations (Hezarkhani, 2006, 2009; Asadi, 2013). Recent studies, including the present work, suggest that mineralization at Chah-Firozeh was controlled by multiple, temporally discrete hydrothermal fluid pulses, resulting in systematic compositional variability in biotite. This study characterizes magmatic and hydrothermal biotite chemistry from the Chah-Firozeh porphyry copper system to constrain ore-forming processes and evaluate the metallogenic fertility of the Kerman Cenozoic Magmatic Arc.

Materials and Methods

In this study, rock samples were analyzed petrographically as thin sections using an Olympus BX60 microscope with Linsky software and a Linkam MDS 600 thermal stage. Based on petrographic observations, four samples were selected for Electron Probe Micro-Analyzer (EPMA) analyses of porphyry indicator minerals (PIMs). Analyses of carbon-coated thin sections were conducted on a JEOL JXA-8200 EPMA at Montanuniversität, with 15 kV, 10 nA, and ~1 μm beam diameter; peak and background times were 100 s and 20 s. Data were processed in OriginPro 6.1 and OriginLab Pro 2024 to produce classification and tectonomagmatic diagrams for interpreting biotite chemistry and potassic alteration in porphyry systems.

Results and Discussion

Magmatic and Potassic Alteration Petrography

The Chah-Firouzeh porphyry copper system provides a well-documented example of the

transition from magmatic mineralogy to hydrothermal alteration assemblages, offering important insights for exploration strategies and vectoring toward mineralization. The magmatic protolith comprises granodiorite–quartz monzonite intrusions dominated by plagioclase, K-feldspar, quartz, and euhedral biotite, subsequently overprinted by hydrothermal alteration.

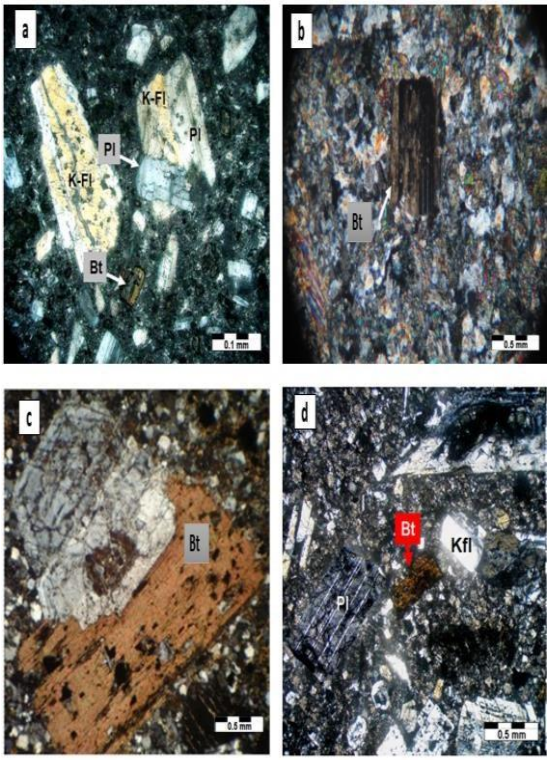

Fig. 2 Photomicrographs showing biotite textures and alteration in the Chah-Firuzeh porphyry copper deposit. (a) Porphyritic granitoid comprising K-feldspar (Kfs), plagioclase (Pl), and biotite (Bt), defining the primary magmatic assemblage. (b) Potassic alteration with Mg-rich biotite and K-feldspar; biotite forms anhedral grains replacing hornblende/biotite and as new phases in groundmass and veinlets. Secondary K- feldspar is present both in veinlets and as replacement of plagioclase. (c) Plagioclase and biotite phenocrysts in a fine quartz-rich groundmass. Potassic alteration shows plagioclase replaced by alkali feldspar. **Abbreviations:** Kfs = K-feldspar; Bt = biotite; Pl = plagioclase.

Petrographic observations reveal that potassic alteration is expressed by the widespread conversion of plagioclase to secondary K-feldspar and by the recrystallization of ferromagnesian minerals, including hornblende and primary biotite, into hydrothermal biotite. The latter occurs as anhedral replacement textures, within vein selvages, and as interstitial phases in the groundmass. Magnetite and quartz are consistently associated, and vein selvages (1.5–4.5 mm wide) commonly host chalcopyrite, pyrite, and molybdenite.

Potassic alteration at Chah-Firouzeh is expressed pervasively in the intrusive core and as vein-controlled selvages, characterized by secondary biotite replacing magmatic mafic phases and K-feldspar forming by plagioclase replacement and veinlet infill (Fig. 2b–d).

Hydrothermal biotite frequently occupies interstitial positions relative to feldspar and quartz, highlighting its late-stage crystallization (Fig.2a-c). These observations indicate that high-temperature potassic alteration at Chah-Firouzeh played a key role in copper mobilization, with its close association with chalcopyrite mineralization defining the potassic zone as the principal exploration target.

Biotite Geochemistry

Biotite, a ferromagnesian silicate, occurs in igneous rocks and porphyry-type ore systems. Its chemical composition provides critical insights into magmatic evolution, hydrothermal alteration, and ore-forming processes. In this study, we present Electron Probe Micro-Analyzer (EPMA) results of magmatic and hydrothermal biotites from the Chah-Firouzeh porphyry copper deposit within the Kerman metallogenic belt. Investigating biotite chemistry is particularly valuable for constraining metallogenic models and guiding exploration strategies in porphyry copper and other magmatic–hydrothermal polymetallic systems.

Biotite chemistry reflects magmatic crystallization and subsequent hydrothermal overprinting. Main factors include fluid composition (H_2O, halogens), metal concentrations, oxidation state, and sulfidation conditions. Additionally, Biotite chemistry reflects melt–fluid–vapor partitioning, volatile exsolution, and complexing under ore-forming temperatures and pressures (Wones et al., 1965; Czamanske et al., 1973; Speer, 1987). Biotite chemistry varies with magmatic differentiation and hydrothermal alteration (Boomeri et al., 2009, 2010; Afshooni et al., 2013; Tang et al., 2019).

Biotite, muscovite, and other micas have been analyzed to infer magmatic and hydrothermal processes (Zhu & Sverjensky, 1991, 1992; et al.). Hydroxyl-bearing micas help estimate HCl and HF fugacities, constraining fluid composition and ore-forming conditions (Munoz, 1984; Finch et al., 1995; Coulson et al., 2001).

Studies of biotite in porphyry copper systems focused on F and Cl as indicators of mineralized versus barren plutons (Parry & Jacobs, 1976; Kesler et al., 1975). Munoz (1984) proposed a model for hydrothermal fluid evolution. In addition, Biotite and phlogopite, containing Fe^{2+}, Fe^{3+}, and OH^-, can be used to assess magmatic conditions (i.e. T (°C), $f(O2)$ and $f(H2O)$) (Yavuz, 2003a).

Table 1. Magmatic biotite analyses from potassic zones, Chah-Firuzeh porphyry copper deposit.

	CHF-1	**CHF-2**	**CHF-3**	**CHF-4**
SiO_2	35.58	35.4	36.63	37.54
TiO_2	2.91	3.25	3.54	3.13
Al_2O_3	13.79	14.03	13.66	14.25
FeO	19.98	20.87	17.42	17.67
MnO	0.33	0.3	0.39	0.44
MgO	10.5	10.04	11.89	11.72
Na_2O	0.04	0.08	0.18	0.08
K_2O	9.11	9.19	8.95	9.67
CaO	0.04	0.02	0.08	0.09
Cr_2O_3	0.03	0.03	0.13	0.1
NiO	0.02	0.07	0.01	0.02
F	0.22	0.21	0.24	0.19
Cl	0.16	0.23	0.19	0.15
Total	92.7	93.69	93.3	95.06
Si	5.86	5.79	5.85	5.92
$Al^{(IV)}$	2.44	2.51	2.45	2.38
$Al^{(VI)}$	0.34	0.3	0.35	0.57
Ti	0.45	0.49	0.53	0.39
Fe^{3+}	0.5	0.53	0.63	0.59
$Al^{(VI)}+Fe^{3+}+$ Ti	1.29	1.32	1.51	1.55
Fe^{2+}	2.34	2.4	1.63	1.89
Mn	0.06	0.06	0.04	0.07
$Fe^{2+}+$ Mn	2.4	2.46	1.67	1.96
Mg	2.58	2.46	2.99	2.66
Ca	0.03	0.02	0.02	0.03
Na	0.02	0.03	0.03	0.03
K	1.85	1.86	1.83	1.86
Total	16.47	16.44	16.35	16.39
^{T}Al	2.78	2.81	2.8	2.95
^{T}Fe	2.84	2.93	2.26	2.48
^{T}Fe + Mn+ Ti+ $Al^{(VI)}$	3.69	3.78	3.18	3.51
F	0.01	0.11	0.13	0.11
Cl	0.05	0.07	0.03	0.03
OH	3.96	3.84	3.87	3.89
X_{Mg}	0.58	0.56	0.68	0.62
X_{Fe}	0.54	0.55	0.44	0.52
X_F	0.01	0.04	0.04	0.03
X_{Cl}	0.02	0.03	0.02	0.02
X_{OH}	0.99	0.94	0.95	0.97
log X_{Cl}/ X_{OH}	-1.69	-1.49	-1.67	-1.68
log X_{F}/ X_{OH}	-1.99	-1.371	-1.371	-1.5
IV (F)	4.73	2.38	2.48	2.58
IV (Cl)	-3.89	-4.02	-3.44	-3.4
IV (F/Cl)	8.67	6.4	5.96	5.99
log(*f*HF/*f*HCl)	-1.08	-1.26	-1.44	-1.54
log(fH_2O/fHF)	7.29	4.97	4.98	5.69
log($fH_2O/fHCl$)	3.79	3.89	3.74	3.93
Temprature (^oC)	706.6	699.46	718.4	694.8

Geochemical Classification of Hydrothermal Biotite

According to the International Mineralogical Association (IMA) classification, biotite is divided into four main end-members: annite, siderophyllite, phlogopite, and eastonite. These classifications are based on differences in their Fe, Mg, Al, and Ti contents. The Mg– (Al^{6I} + Fe^{3+} + Ti)– (Fe^{2+} + Mn) and (Mg–Li)– (Fe_{tot} + Mn + Ti − Al^{6I}) diagrams effectively discriminate magmatic from hydrothermal biotite in the Chah-Firouzeh porphyry copper deposit.

Using the Foster (1960) system, refined by Tischendorf et al. (1997), potassic alteration and primary magmatic biotite consistently plot in the Mg–Fe fields (Fig. 3a–b). Mg-rich biotite (Mg- to Fe-biotite) is common in other porphyry copper and polymetallic deposits and serves as a key indicator of porphyry-related magmatic– hydrothermal mineralization.

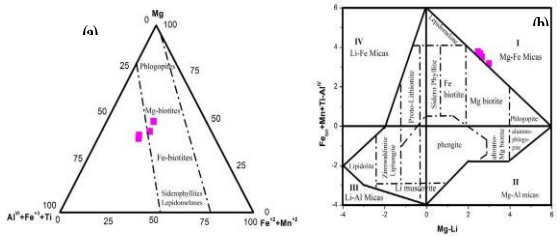

Fig. 3 Biotite compositions from Chah-Firuzeh plotted on Foster (1960) Mg–Fe–Ti and Tischendorf et al. (1997) Mg–Li discrimination diagrams.

Geo-Thermometry

Biotite Ti content is highly sensitive to temperature and oxygen fugacity, making it a reliable geothermometer for igneous and metamorphic rocks (Robert, 1976; Patino Douce, 1993). Biotite Ti and Mg/ (Mg + Fe) were used to estimate crystallization temperatures via Henry et al. (2005) calibration (Fig. 4a).

Ti-in-biotite geothermometry indicates magmatic biotite from Chah-Firuzeh crystallized at ~700–722 °C. Ti-in-biotite temperatures (°C) were calculated from Ti (apfu) and X_{Mg} using Henry et al. (2005) calibration, valid for Ti 0.39–0.53 apfu, X_{Mg} 0.56–0.68.

The chemical variations observed in biotite have traditionally been employed to estimate both the high-temperature conditions and oxygen fugacity in magmatic environments (Wones and Eugster., 1965). Biotite from the potassic zone of the Chah-Firouzeh deposit reflect lower temperatures (~394–418 °C, Fig. 4a). Fig. 4b compares Ti content (apfu) with values predicted by the geothermometer. Biotite remains stable between ~695–718 °C, with Ti contents approaching ~0.5 apfu near the lower limit.

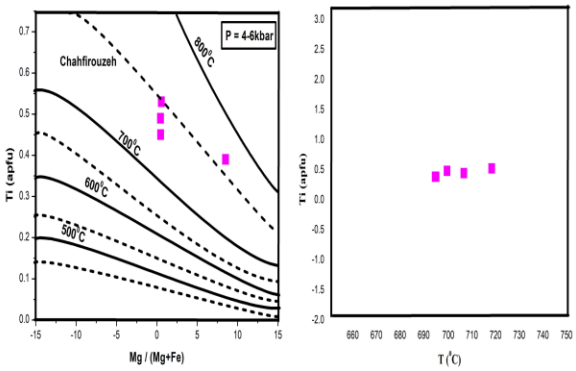

Fig. 4 shows biotite temperatures from Ti–Mg/ (Mg + Fe) calibration (a, °C) and Ti content (apfu) versus temperature (b) following Henry et al. (2005) and Edgar & Artur (2024).

Oxidation State (fO_2) in Magmas

Wones and Eugster (1965) showed that biotite's magnesium number [X_{Mg} = Mg/(Mg + Fe)] rises with higher oxygen or sulfur fugacity, as oxidizing conditions increase Fe^{3+}/Fe^{2+} in melts, limiting Fe^{2+} competition with Mg^{2+} in octahedral sites. High oxygen fugacity raises X_{Mg} in biotite and mafic minerals, making Mg-rich compositions indicators of oxidized magmas. In addition, Wones et al. (1965) showed biotite compositions on the Fe^{2+}–Fe^{3+}–Mg ternary diagram aligns with quartz–fayalite–magnetite (QFM), nickel–nickel oxide (NNO), and hematite–magnetite (HM) (Fig. 5). Mineral proxies for oxygen fugacity are widely used in granitic and porphyry systems (e.g., Loferski et al., 1995; Li et al., 2007; Zhang et al., 2016).

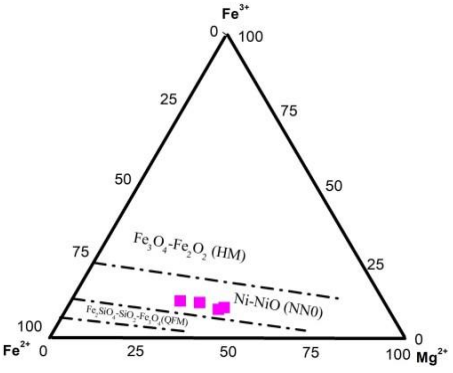

Fig. 5 Biotite from Chah-Firuzeh plotted on the Fe^{3+}–Fe^{2+}–Mg ternary diagram, showing redox trends (Wones et al., 1965).

Magmatic and hydrothermal biotite from Chah-Firouzeh plot at or above the NNO buffer, reflecting high oxygen fugacity crystallization. The Mg number (X_{Mg}) of biotite from this zone ranges from 0.56 to 0.68, reflecting Mg-rich compositions characteristic of oxidized magmatic–hydrothermal systems. In addition, Biotite Fe^{3+}/Fe^{2+} ratios (0.22–0.31) decrease from hydrothermal to magmatic, indicating rising oxygen fugacity from magmatic to hydrothermal stages. Redox conditions intensified progressively during potassic alteration in the Chah-Firouzeh porphyry system.

High fO_2 promotes porphyry and epithermal mineralization by favoring sulfur as SO_4^{2-} and SO_2 in melts. Under such High fO_2 suppresses magmatic sulfides, concentrating Cu in the melt and hydrothermal fluid, enhancing Cu mineralization (Xiong et al., 2001; Li et al., 2008). Molybdenum mineralization is commonly associated with oxidized felsic granitoid magmas (Mengason et al., 2011).

The fluids responsible for porphyry Cu–(Mo–Au) mineralization are generally considered moderately to highly oxidized, with fO_2 conditions ranging between the nickel–nickel oxide (NNO) and hematite–magnetite (HM) buffers (Burnham et al., 1980; Afshooni et al., 2013). For Example, Deboullie crystallized at NNO (Loferski et al., 1995), Kahang and Darreh-Zar at HM–NNO (Afshooni et al., 2013; Parsapoor et al., 2015)., suggesting Chah-Firouzeh formed above NNO, with fO_2–T variations aiding Cu enrichment (Fig. 5).

Petrogenesis and Tectonic Setting

Biotite chemistry reveals tectono-magmatic processes and granite petrogenesis, reflecting temperature, fO_2, pressure, and tectonic setting (Speer, 1981; Ague et al., 1988; Abdel-Rahman, 1994; Zhou, 1986)). Biotite in granites stores excess Al in the absence of garnet, cordierite, or Al_2SiO_5, reflecting magma per-aluminosity and oxidation state (Shabani et al., 2003).

Biotite ASI mirrors host granite ASI, highlighting its role as the main reservoir for excess aluminum in granitic systems (De Albuquerque, 1973; Lalonde et al., 1993). Biotite composition tracks granite type: Fe-rich in A- type, Mg-rich in I-type, Al-rich in S-type; Mg and oxidation indices effectively distinguish I- from S-type granites (Abdel-Rahman, 1994; Xu et al., 1986).

Biotite-based diagrams Fe/(Fe+Mg) vs F (Dahlquist et al., 2010), Al^{4}–$Fe^{2+}/(Fe^{2+}+Mg)$ (Jiang et al., 2002), and $MgO–FeO_{tot}–Al_2O_3$ (De Albuquerque, 1973) distinguish granite types (A, I, S-types) and coexisting minerals (amphibole, muscovite, or Al-silicates (sillimanite). Nachit et al. (1985) Al–Mg diagram classifies granites, while biotite IV(F) values reflect magmatic affinity: calc-alkaline high, high-K calc-alkaline intermediate, alkaline low, peraluminous broad (Sallet, 2000). Biotite compositions plot a continuum from Mg-rich, Al-poor magnetite-series to Fe- and Al-rich ilmenite-series granites on Fe/(Fe+Mg)–Al diagrams (Zemanski et al., 1981; Lalonde et al., 1993).

In the Maherabad, Dehnow, and Najmabad plutons, $TiO_2–Al_2O_3$ biotite data show magnetite-series granites have high TiO_2/low Al_2O_3, while ilmenite-series have low TiO_2/high Al_2O_3 (Karimpour, 2011). Zhou (1986) showed that w(∑FeO)/[w(∑FeO) +w(MgO)] vs w(MgO) biotite plots distinguish crustal, crust–mantle, and mantle-derived granite sources worldwide.

Abdel-Rahman (1994) used $MgO–FeO_{tot}–Al_2O_3$ biotite diagrams of 325 samples to differentiate anorogenic, calc-alkaline, and peraluminous (S-type) granite tectonic settings. Ague et al. (1988) showed biotite log (X_F/X_{OH}) vs log (X_{Mg}/X_{Fe}) plots reveal crustal contamination in I-type granites, classified as (I-SC), moderately contaminated (I-MC), weakly contaminated (I-WC), or strongly contaminated and reduced (I-SCR) types.

Biotite aids granite petrogenesis and tectonic studies but is best combined with geochemistry, isotopes, and regional geology; Chah-Firuzeh magmatic biotites plot in calc-alkaline to peraluminous fields (Abdel-Rahman, 1994; Hu et al., 2006). Chah-Firuzeh biotites plot in the crust–mantle mixed-source field on w(∑FeO)/[w(∑FeO) +w(MgO)] vs w(MgO) diagrams (Fig.6a and 6b), consistent with geochemistry and zircon Hf data (Abdel-Rahman, 1994; Zhou, 1986; Leng et al., 2016).

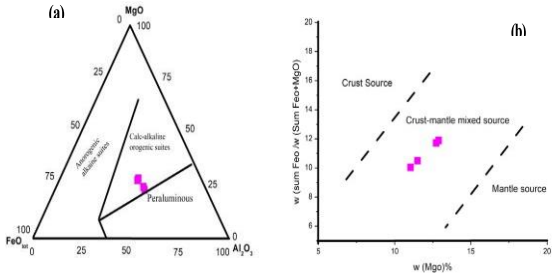

Fig. 6 Chah-Firuzeh biotites on (a) MgO– $FeO_{tot}–Al_2O_3$ ternary diagram for tectono- magmatic affinity (after Abdel-Rahman, 1994) and (b) w(ΣFeO)/[w(ΣFeO)+w(MgO)] vs w(MgO) (after Zhou, 1986) for magma source.

Halogen Chemistry

Biotite halogens: Biotite hosts 70–90% of F in fluorite-free granitoids, with F and Cl substituting for

OH; Cl content is lower due to its larger ionic radius (Speer, 1984; Zhang et al., 2016; Munoz, 1984). Cl in biotite rises in Cl-rich magmas or fluids; high Mg/Fe favors F, low Mg/Fe favors Cl, though Darreh-Zar, Kahang, Dalli, and Casino biotites deviate from these trends (Munoz, 1984; Parsapoor et al., 2015; Afshooni et al., 2013). At Chah-Firuzeh, biotite F rises with X_{Mg}, following "F–Fe avoidance," while Cl shows no X_{Mg} trend, indicating crystallization from hydrothermal fluids with distinct halogen signatures (Fig. 7a and b).

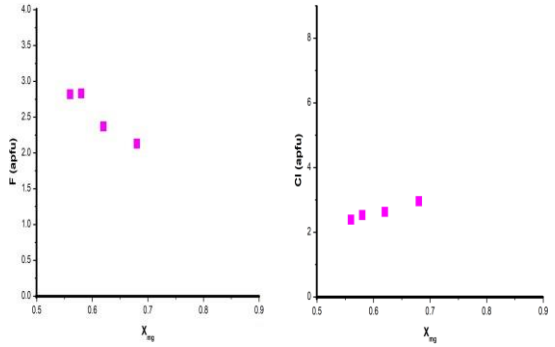

Fig. 7 Biotite halogens in Chah-Firuzeh: F content (apfu) versus Mg mole fraction (XMg).

Zhu and Sverjensky (1992) showed biotite formed under similar conditions plots linearly on log (X_F/X_{OH}) vs XFe and log (X_{Cl}/X_F) vs X_{Fe}, with slopes depending on temperature. Chah-Firuzeh potassic biotites show log (X_F/X_{OH}) −1.37 to −1.99 and log (X_{Cl}/X_{OH}) −1.49 to −1.69; slopes for log (X_{Cl}/X_{OH})–X_{Mg} and log (X_F/X_{OH})–X_{Fe} were calculated at 316–420 °C using Zhu and Sverjensky (1992).The Chah-Firuzeh potassic biotites have log (X_F/X_{OH}) −1.37 to −1.99 and log (X_{Cl}/X_{OH}) −1.49 to −1.69; slopes on log (X_F/X_{OH})–X_{Fe} and log (X_{Cl}/X_{OH})–X_{Mg} plots are −1.69 and 0.56, showing distinct hydrothermal biotite types (Fig. 8a–b).

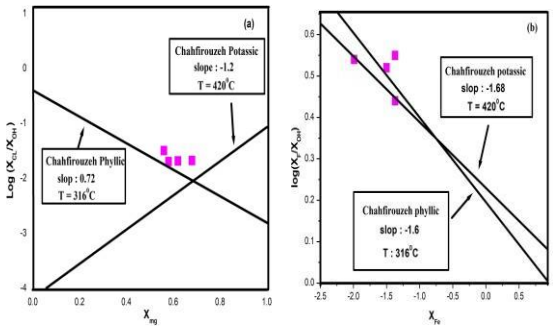

Fig. 8 Chah-Firuzeh biotite halogens: X_{Mg} vs log (X_{Cl}/X_{OH}) and X_{Fe} vs log (X_F/X_{OH}) showing hydrothermal variation and slope trends.

Selby and Nesbitt (2000) noted that biotite from Casino's potassic zone shows consistent halogen ratios, reflecting stable fluid composition and temperature. In contrast, Chah-Firuzeh biotite displays variable halogen ratios, recording changing fluid chemistry during crystallization. Munoz (1984) highlighted IV(F), IV(Cl), and IV(F/Cl) as key parameters for biotite F and Cl content, reflecting the *f*(HCl)/*f*(HF) ratio. Munoz (1984) defined biotite halogen intercepts as:

$$\mathrm{IV(F)} = 1.5X_{\mathrm{Mg}} + 0.42X_{\mathrm{ann}} + 0.20X_{\mathrm{sid}} - \log\left(\frac{X_F}{X_{\mathrm{OH}}}\right)$$

$$\mathrm{IV(Cl)} = -5.01 - 1.93X_{\mathrm{Mg}} - \log\left(\frac{X_{\mathrm{Cl}}}{X_{\mathrm{OH}}}\right)$$

$$\mathrm{IV(F/Cl)} = \mathrm{IV(F)} - \mathrm{IV(Cl)}$$

where $X_{\mathrm{sid}}$and $X_{\mathrm{ann}}$are the biotite mole fractions of siderophyllite and annite, respectively (Yavuz, 2003).

$$X_{\mathrm{sid}} = \frac{3 - (\mathrm{Si/Al})}{1.75} \times (1 - X_{\mathrm{Mg}})$$

$$X_{\mathrm{ann}} = 1 - (X_{\mathrm{Mg}} - X_{\mathrm{sid}})$$

These parameters quantify F and Cl in biotite, reflecting crystal chemistry and *f*(HCl)/*f*(HF). Lower IV(F) indicates F enrichment, more negative IV(Cl) indicates Cl enrichment, and lower IV(F/Cl) corresponds to higher F/Cl. IV(F/Cl) is temperature-independent, minimally affected by OH occupancy, and directly tracks fluid fugacity, making it a robust fluid indicator. Applied to porphyry deposits, IV systematics show Cu systems are Cl-rich, Mo systems F-rich (Munoz, 1984; Yavuz, 2003). Chah-Firuzeh biotite shows IV(F) 2.38–4.73, IV(Cl) 4.02 to 3.49, IV(F/Cl) 5.96–8.67 (Table 1); on the IV(F/Cl)–IV(F) plot, values fall in the porphyry Cu field (Fig. 9), indicating Cl-rich hydrothermal fluids.

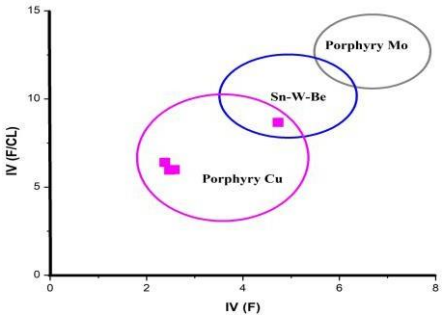

Fig. 9 Chah-Firuzeh biotite IV(F/Cl) vs IV(F) diagram showing F–Cl systematics and fluid characteristics (after Munoz, 1984; Boomeri et al., 2009).

The Chah-Firuzeh system is F-enriched, with abundant fluorite and pervasive Mg-rich biotite typical of porphyry Cu rocks. Cl enrichment is limited by biotite chemistry and ionic radii (Cl^- 1.81 Å vs F^- 1.31 Å/OH^- 1.38 Å), so even trace Cl indicates Cl-rich melts or fluids (Munoz, 1984; Taylor, 1983; Selby & Nesbitt, 2000; Boomeri et al., 2010; Afshooni et al., 2013).

Porphyry Cu vs. Mo dominance depends on source composition, magma H_2O and volatiles (F/Cl, F/H_2O), tectonics, emplacement depth, fO_2, vapor timing, and metal content. High F, F/Cl, and F/H_2O in Mo magmas may reflect source inheritance or metamorphic dehydration; early vapor saturation can raise F/Cl by removing Cl, Cu, and Mo to the vapor (Beane et al., 1981; Hannah et al., 1990; Loferski et al., 1995; Candela & Holland, 1984). Porphyry Cu biotites record high Cl/F, reflecting Cl- and alkali-rich magmatic fluids from intermediate magmas in upper-crust convergent settings; high Cl indicates magmas were not vapor-saturated early, which otherwise removes Cu via Cl-bearing vapor (Burnham & Ohmoto, 1980; Sillitoe & Khan, 1977; Candela & Holland, 1984).

Halogen fugacity: Fluorine and chlorine control magmatic–hydrothermal systems by affecting vapor saturation, metal complexing, fluid composition, and mineralization style. Halogen fugacity ratios were calculated using Munoz (1992) formulations, based on F–Cl–OH exchange in biotite–melt/fluid equilibria and biotite composition models (Zhu & Sverjensky, 1991, 1992), providing a robust framework to quantify halogen behavior in magmatic–hydrothermal systems (Munoz & Ludington, 1974; Munoz, 1984, 1992; Selby et al., 2000).

Fluid halogen fugacities were calculated from biotite–fluid equilibria:

$$\log\left(\frac{f_{H_2O}}{f_{HF}}\right)_{fluid} = \frac{1000}{T}\left[2.37 + 1.1(X_{phl})_{biotite}\right] + 0.43 - \log\left(\frac{X_F}{X_{OH}}\right)_{biotite}$$

$$\log\left(\frac{f_{H_2O}}{f_{HCl}}\right)_{fluid} = \frac{1000}{T}\left[1.15 + 0.55(\ )_{phl\ biotite}\right] + 0.68 - \log\left(\frac{X_{Cl}}{X_{OH}}\right)_{biotite}$$

$$\log\left(\frac{f_{HF}}{f_{HCl}}\right)_{fluid} = -\frac{1000}{T}\left[1.22 + 1.65(X_{phl})_{biotite}\right] + 0.25 + \log\left(\frac{X_F}{X_{Cl}}\right)_{biotite}$$

where T is the temperature (in Kelvin) X_{phl} is the phlogopite fraction (Mg octahedral sites), and X_F, X_{Cl}, and $X_{OH}$are biotite hydroxyl-site mole fractions.

Magmatic and hydrothermal biotites from Chah-Firuzeh show distinct halogen fugacity ratios: magmatic biotite has log(fHF/fHCl) −1.08 to −1.54, log(fH₂O/fHCl) 3.74–3.93, and log(fH₂O/fHF) 4.97–7.29, whereas hydrothermal biotite shows lower fHF/fHCl and higher fH₂O/halogen ratios. This shift reflects cooling-driven evolution from halogen-rich magma to water-dominated hydrothermal fluids, halogen dilution during fluid exsolution, and partial overprinting of primary magmatic signatures rather than a single homogeneous fluid (Fig. 10a–b).

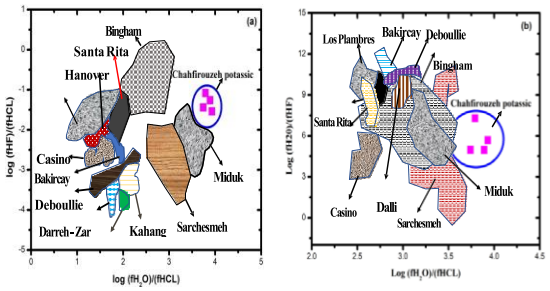

Fig. 10 (a) log(fHF/fHCl) vs. log(fH₂O/fHCl) and (b) log(fH₂O/fHCl) vs. log(fH₂O/fHF) for Chah-Firuzeh biotites, showing magmatic- to-hydrothermal fluid evolution during potassic alteration (after Selby et al., 2000).

Increasing H_2O during magmatic–hydrothermal evolution raises biotite log (fH₂O/fHCl) and log (fH₂O/fHF); extreme values reflect post-entrapment modification by meteoric fluids (Selby and Nesbitt, 2000). Hydrothermal biotites from the potassic zone with high log (fH₂O/fHCl) and log (fH₂O/fHF) reflect formation from fluids variably mixed with meteoric water. Fluid ascent and rapid cooling–decompression drive acidification, early silicate alteration, and subsequent sulfide precipitation during progressive neutralization. Continued halogen dilution by fluid evolution and meteoric input produces elevated halogen water ratios preserved in biotite.

The Chah-Firozeh system preserves a magmatic-to-hydrothermal transition reflected by biotite chemistry. Fe–Mg–rich hydrothermal biotite reflects high-T, oxidizing conditions favorable for Cu–Mo mineralization. The calculated Fe^{3+}/Fe^{2+} ratios, with X_{Fe} and X_{Mg} indicate biotite crystallization above the nickel–nickel oxide NNO buffer, consistent with oxidized arc magmas (Wones and Eugster, 1965). High IV(F/Cl) ratios (5.9–8.7) indicate F-rich, oxidized hydrothermal fluids during biotite growth.

Deviations from Mg–Cl trends reflect late fluid modification by dilution or meteoric

mixing, with Cu transport favored by fluoride or sulfate complexes rather than chloride species. Biotite chemistry indicates a high-fO_2, F-rich calc-alkaline magmatic source typical of arc-related porphyry systems.

At Chah-Firozeh, calc-alkaline I- type magmas and biotite Fe–Mg–Al systematics reflect subduction origin and magma hybridization during ascent. Early high-temperature potassic alteration and biotite growth mark ore initiation, followed by cooling and declining fO_2 that drive sulfide precipitation.

Copper in Biotite

Biotite Cu reflects magmatic fertility, with barren intrusions low in Cu and mineralized systems much higher (Parry et al., 1963). Biotite Cu can indicate magmatic metallogenic potential, increasing during early crystallization and declining as Cu partitions into hydrothermal fluids (Grabeal, 1973). However, some barren intrusions show higher biotite Cu than mineralized zones (Hendry et al., 1981, 1985).

Cu is extracted from mafic minerals in fertile systems but retained in barren intrusions, with Late Cretaceous biotites averaging ~700 ppm Cu (Al-Hashimi et al., 1970). Extremely high Cu in biotite often reflects sub-microscopic Cu-bearing mineral inclusions (chalcopyrite, bornite, cuprite) rather than lattice substitution.

Transmission electron microscopy (TEM) studies show these inclusions, mostly 2–100 nm thick and up to ~1000 nm wide, occupy interlayers and lie parallel to biotite sheets (Ilton and Veblen, 1988, 1993). Cu-rich inclusions form preferentially in deformed or expanded biotite interlayers, emphasizing structural control on Cu hosting.

Post-magmatic processes, including weathering, can further enrich Cu, as seen in altered Lakeshore biotite (0.16–8.86 wt%; Cook, 1988) and Cyprus Casa Grande biotite, where Cu occurs in expanded interlayers and native inclusions (Ilton and Veblen, 1993). Distinguishing primary magmatic–hydrothermal Cu from supergene enrichment is essential.

Biotite Cu reflects magmatic differentiation, fluid evolution, and ore formation, with Mg–Fe–rich biotites in systems like Chah- Firozeh aiding Cu transport and deposition.

Biotite Cu variability reflects both structural incorporation and nano- to microscale inclusions, requiring detailed petrographic and microanalytical study when using Cu as an exploration vector.

Biotite Chemistry as a Magmatic Fertility Indicator

Biotite composition reflects magmatic conditions controlling porphyry system fertility. Ore-associated biotites are Mg-rich, Fe-poor (Mg/Fe >0.5), Ti-enriched (TiO_2 >3 wt%), Al- and Na-depleted (Al_2O_3 <15 wt%, CaO <0.5 wt%), K-rich (K/Na >10), and enriched in volatile and metal- related elements (Ba, Cu, F, Cl).

These features indicate crystallization from high-T, oxidized, volatile-rich magmas, with biotite redox providing key constraints on ore-forming processes. For example, Mineralization-related biotites form under high oxygen fugacity, enhancing chalcophile element mobility (Qin, 2009).

In the Sisson Brook W–Mo–Cu system, granitic dykes with biotite equilibrated near the NNO buffer, likely sourcing ore-forming fluids (Zhang et al., 2016). In contrast, less evolved plutons near the QFM buffer are relatively barren, highlighting the role of magmatic differentiation and oxidation in fertility.

Biotite halogens track fluid evolution: progressive Cl depletion during magma evolution partitions Cl into exsolved, metal-rich fluids, as seen in Cl–Sn– bearing biotite at the Furong deposit (Li et al., 2007). Similarly, F-rich biotites reflect distinct physicochemical conditions in uranium-bearing granites. Lower-T, low-fO_2, peraluminous magmas favor U enrichment (Chen et al., 2010; Zhang et al., 2011), while high-T, F-rich, moderately oxidized biotites at Ziyunshan support U–W mineralization (Tang et al., 2016).

Biotite from the Chah-Firozeh deposit reflects high ore-forming potential, with granitic rocks showing fO_2 above NNO, advanced differentiation, and Cl depletion indicating efficient volatile exsolution and metal transfer. Mg/Fe >0.5, TiO_2 >3 wt%, Al_2O_3 <15 wt%, high K/low Na, and Ba, Cu, F, Cl enrichment mark conditions favorable for porphyry mineralization. Combined with petrography and whole-rock geochemistry, biotite chemistry robustly constrains magmatic oxidation, volatile budget, and metallogenic fertility.

Biotite chemistry and porphyry fertility: Biotite is a key indicator in porphyry systems, with Mg–Fe–rich assemblages commonly associated with high-grade Cu (Sillitoe & Richards, 2015). Its composition reflects temperature, fO_2, and fluid chemistry, reflecting

magmatic–hydrothermal evolution and guiding exploration. In Chahfirouzeh, Mg–Fe-rich biotite reflects high-T, moderately oxidized magmas capable of Cu transport.

These biotites equilibrate with potassic alteration and Cu-bearing sulfides (chalcopyrite, bornite), indicating 500–700 °C conditions from a thermally sustained magmatic source. Their distribution and chemistry trace hydrothermal processes and guide exploration of high-grade Cu zones.

Magmatic–Hydrothermal Evolution

F- and Mg-rich biotites reflect crystallization from high-temperature, moderately oxidized magmas, highlighting volatile-rich conditions that enhance Cu transport and delay sulfide saturation. Their chemistry reflects high oxygen fugacity typical of fertile porphyry copper systems. In contrast, the relatively limited incorporation of Cl into biotite suggests that chloride partitioning into the solid phase was minor, implying that Cl was preferentially concentrated in the coexisting magmatic hydrothermal fluid or that its role in metal transport was secondary during the main stages of mineralization.

Under such conditions, copper precipitation was likely governed by alternative physicochemical triggers, including shifts in fluid pH, cooling-induced changes in metal solubility, or redox-driven sulfate sulfide transitions that promoted sulfide saturation and Cu deposition. Together, these features indicate a magmatic–hydrothermal system in which oxidation state, volatile composition, and fluid evolution collectively controlled the timing and efficiency of copper mineralization.

Magma classification and tectonic implications: Biotite major-element chemistry constitutes a sensitive tracer of both tectonomagmatic regime and magmatic evolution. In subduction-related, calc-alkaline magmatic systems, biotite typically exhibits elevated Mg and Al_2O_3 contents, consistent with crystallization from H_2O-rich, relatively oxidized melts characteristic of arc environments.

By contrast, biotite compositions enriched in Fe are more characteristic of collisional to post-collisional magmatic regimes, where melts are typically more evolved and redox conditions are comparatively variable. Parameters such as Mg/ (Mg + Fe) and Ti abundance serve as additional petrogenetic indicators, reflecting relative crystallization temperatures and facilitating discrimination between calc-alkaline and tholeiitic magma series.

Halogen systematics in biotite further reflect the volatile budget of the parental melt: Elevated F contents are indicative of crystallization from F-rich, H_2O-bearing magmas, whereas increased Cl concentrations may reflect interaction with saline magmatic fluids or exsolved hydrothermal brines. Collectively, these geochemical attributes demonstrate that biotite functions as an effective mineral proxy for constraining magma physicochemical parameters, tectonomagmatic affinity, and the nature and evolution of associated fluid phases within igneous and hydrothermal environments (Tischendorf et al., 2001; Wones & Eugster, 1965; Abdel-Rahman, 1994).

Conclusion

Electron-microprobe analyses of biotite from the potassic alteration zone of the Chah-Firozeh porphyry Cu deposit identify two genetically distinct populations of magmatic and hydrothermal origin. Magmatic biotite crystallized at ~700–720
°C under strongly oxidizing conditions ($fO_2 \geq$ NNO, approaching HM), consistent with an oxidized, Cu- fertile magmatic system.

Hydrothermal biotite is Mg–Fe-rich and enriched in F, reflecting multiple high-temperature, F-rich fluid pulses during potassic alteration. Biotite halogen fugacity ratios (log fH_2O/fHF = 4.9–7.3; log $fH_2O/fHCl$ = 3.7–3.9) indicate evolving magmatic– meteoric fluid interaction, while halogen systematics conform to Fe–F avoidance and variable Cl partitioning.

These compositional features demonstrate that biotite chemistry effectively discriminates mineralized from barren intrusions and constrains magma oxidation state, fluid evolution, and tectonomagmatic setting, supporting formation from oxidized, calc-alkaline magmas in a subduction- related environment favorable for porphyry Cu mineralization.

Acknowledgement

This study is part of the M.Phil. thesis of Johar Ali at Shiraz University, Iran. We thank colleagues and the Research and Development Center of the National Iranian Copper Industries Company (NICICo) for field support at the Chah-Firuzeh deposit. Special thanks are due to Dr. Sina Asadi for electron microprobe data, samples, and guidance, Dr. Arezou Al-Sadat Mir Bagheri Dehaghani are thanked for manuscript review, and Prof. S. Asadi for constructive feedback that improved the study's clarity and quality.

Statements and Declarations

Funding: Financial support for this investigation was provided by the Department of Earth Sciences, School of Science, University of Shiraz, Iran (Grant No. 1GRC1M236280).

Competing Interests: The authors declare that there are no financial, professional, or personal conflicts of interest related to this research.

Author's contributions: All authors contributed to the development of the study concept and research design. Johar Ali was responsible for sample preparation, data acquisition, and analytical work. The initial manuscript was prepared by Johar Ali, Sina Asadi, and Arezou Al- Sadat Mir, while Bagheri Dehaghani provided critical revisions and feedback on earlier drafts. Each author reviewed the final version of the manuscript and approved it for publication.

Data availability: All data generated or analyzed during this study are included in the submitted manuscript.

References

Abdel-Rahman, A. M. (1994). Characterization of biotite in alkaline, calc-alkaline, and peraluminous magmas. *Journal of Petrology*, **35**(2), 525–541. https://doi.org/10.1093/petrology/35.2.525

Afshooni, S. Z., Mirnejad, H., Esmaeily, D., Haroni, H. A. (2013). The Hydrothermal biotite geochemistry in the Kahang porphyry copper deposit, northeastern Isfahan, Iran. *Ore Geology Reviews*, **54**, 214–232. https://doi.org/10.1016/j.oregeorev.2013.03. 003

Ague, J. J., Brimhall, G. H. (1988). Regional variations in bulk chemistry, mineralogy, and mafic mineral compositions in the California batholith. *Geological Society of America Bulletin*, **100**, 891–911. https://doi.org/10.1130/0016-7606(1988)100

Alavi, M. (1980). Tectonostratigraphic development of the Zagros orogenic belt, Iran. *Geology*, **8**(3), 144–149. https://doi.org/10.1130/0091- 7613(1980)8

Al-Hashimi, A. R. K., Brownlow, A. H. (1970). Copper concentration in biotites from the Boulder Batholith, Montana. *Economic Geology*, **65**(8), 985–992. https://doi.org/10.2113/gsecongeo.65.8.985

Asadi, S. (2013). Geochemistry of selected productive and barren intrusions in Shahr Babak copper complex, Urumiyeh–Dokhtar volcano–magmatic belt (Doctoral dissertation, Shiraz University).

Asadi, S., Mathur, R., Moore, F., Zarasvandi, A. (2015). Copper isotope fractionation in the Meiduk porphyry copper deposit, northwest of the Kerman Cenozoic magmatic arc, Iran. *Terra Nova*, **27**(1), 36–41. https://doi.org/10.1111/ter.12135

Asadi, S., Moore, F., Zarasvandi, A. (2014). Discriminating productive and barren porphyry copper deposits in the southeastern part of the Central Iranian volcano–plutonic belt, Kerman region, Iran: A review. *Earth-Science Reviews*, **138**, 25–46. https://doi.org/10.1016/j.earscirev.2014.08.002

Beane, R. E. (1974). The biotite stability in the porphyry copper environment. *Economic Geology*, **69**(2), 241–256. https://doi.org/10.2113/gsecongeo.69.2.241

Berberian, F., Muir, I. D., Pankhurst, R. J., Berberian, M. (1982). Late Cretaceous and early Miocene Andean-type plutonic activity in northern Makran and central Iran. *Journal of the Geological Society*, **139**(5), 605–614. https://doi.org/10.1144/gsjgs.139.5.0605

Boomeri, M., Nakashima, K., Lentz, D. R. (2009). The Miduk porphyry Cu deposit, Kerman, Iran: A geochemical analysis of the potassic zone including halogen element systematics related to Cu mineralization processes. *Journal of Geochemical Exploration*, **103**(1), 17–29. https://doi.org/10.1016/j.gexplo.2009.05.002

Boomeri, M., Nakashima, K., Lentz, D. R. (2010). The Sarcheshmeh porphyry copper deposit, Kerman, Iran: A mineralogical analysis of the igneous rocks and alteration zones including halogen element systematics related to Cu mineralization processes. *Ore Geology Reviews*, **38**(4), 367–381. https://doi.org/10.1016/j.oregeorev.2010.08. 001

Burnham, C. W., Ohmoto, H. (1980). Late-stage processes of felsic magmatism. *Economic*

Geology, **75**(1), 1–24.

Candela, P. A., Holland, H. D. (1984). The partitioning of copper and molybdenum between silicate melts and aqueous fluids. *Geochimica et Cosmochimica Acta*, **48**(2), 373–380. https://doi.org/10.1016/0016-7037(84)90257-6

Coulson, I., Dipple, G., Raudsepp, M. (2001). Evolution of HF and HCl activity in magmatic volatiles of the gold-mineralized Emerald Lake pluton, Yukon Territory, Canada. *Mineralium Deposita*, **36**(6), 594–606. https://doi.org/10.1007/s0012600179

Czamanske, G. K., Wones, D. R. (1973). Oxidation during magmatic differentiation, Finn Marka complex, Oslo area, Norway: Part 2, the mafic silicates. *Journal of Petrology*, **14**(3), 349–380. https://doi.org/10.1093/petrology/14.3.349

Czamanske, G. K., Ishihara, S., Atkin, S. A. (1981). Chemistry of rock-forming minerals of the Cretaceous-Paleocene batholith in southwestern Japan and implications for magma genesis. *Journal of Geophysical Research: Solid Earth*, **86**(B11), 10431– 10469. https://doi.org/10.1029/JB086iB11p10431

Dahlquist, J. A., Alasino, P. H., Eby, G. N., Galindo, C., Casquet, C. (2010). Fault-controlled Carboniferous A-type magmatism in the proto-Andean foreland (Sierras Pampeanas, Argentina): Geochemical constraints and petrogenesis. *Lithos*, **115**(1–2), 65–81. https://doi.org/10.1016/j.lithos.2009.12.007

De Albuquerque, C. A. (1973). Geochemistry of biotites from granitic rocks, northern Portugal. *Geochimica et Cosmochimica Acta*, **37**(7), 1779–1802. https://doi.org/10.1016/0016-7037(73)90162-3

Finch, A. A., Parsons, I., Mingard, S. C. (1995). Biotite compositions as indicators of fluorine activity in late-stage magmatic fluids: Insights from the Gardar Province, South Greenland. *Journal of Petrology*, **36**(6), 1701–1728. https://doi.org/10.1093/petrology/36.6.1701

Foster, M. D. (1960). Interpretation of trioctahedral mica compositions, (U.S. Geological Survey Professional Paper 354-B). U.S. Government Printing Office.

Graybeal, F. T. (1973). Copper, manganese, and zinc in co-existing mafic minerals from Laramide intrusive rocks in Arizona. *Economic Geology*, **68**(6), 785–798. https://doi.org/10.2113/gsecongeo.68.6.785

Hendry, D., Chivas, A. R., Long, J., Reed, S., (1985). Chemical differences between minerals from mineralizing and barren intrusions from some North American porphyry copper deposits. *Contributions to Mineralogy and Petrology*, **89**(4), 317–329. https://doi.org/10.1007/BF00379460

Hendry, D., Chivas, A. R., Reed, S., Long, J., (1981). Geochemical evidence for magmatic fluids in porphyry copper systems. *Contributions to Mineralogy and Petrology*, **78**(4), 404–412. https://doi.org/10.1007/BF00398919

Henry, D. J. (2005). The Ti-saturation surface for low- to medium-pressure metapelitic biotites: Implications for geothermometry and Ti- substitution mechanisms. *American Mineralogist*, **90**(2–3), 316–328. https://doi.org/10.2138/am.2005.1498

Hezarkhani, A. (2006). Hydrothermal evolution of the Sar-Cheshmeh porphyry Cu–Mo deposit, Iran: Evidence from fluid inclusions. *Journal of Asian Earth Sciences*, **28**(4–6), 409–422. https://doi.org/10.1016/j.jseaes.2006.03.002

Hezarkhani, A. (2009). Hydrothermal fluid geochemistry at the Chah-Firuzeh porphyry copper deposit, Iran: Evidence from fluid inclusions. *Journal of Geochemical Exploration*, **101**(3), 254–264. https://doi.org/10.1016/j.gexplo.2009.01.002

Hu, J., Qiu, J. S., Wang, R. C., Jiang, S. Y., Xing, H. F., Wang, X. L. (2006). Zircon U–Pb geochronology, biotite mineral chemistry, and their petrogenetic

implications of the Longwo and Baishigang plutons in Guangdong Province. *Acta Petrologica Sinica*, **22**(10), 2464–2474.

Ilton, E. S., Veblen, D. R. (1993). Origin and mode of copper enrichment in biotite from rocks associated with porphyry copper deposits: A transmission electron microscopy investigation. *Economic Geology*, **88**(4), 885–900. https://doi.org/10.2113/gsecongeo.88.4.885

Jacobs, D. C., Parry, W. T. (1976). A comparison of the geochemistry of biotite from some Basin and Range stocks. *Economic Geology*, **71**(6), 1029–1035. https://doi.org/10.2113/gsecongeo.71.6.1029

Jiang, Y., Jiang, S., Ling, H., Zhou, X., Rui, X., Yang, W. (2002). Petrology and geochemistry of shoshonitic plutons from the western Kunlun orogenic belt, Xinjiang, northwestern China: Implications for granitoid genesis. *Lithos*, **63**(3), 165–187. https://doi.org/10.1016/S0024-4937(02)00124-4

Karimpour, M. H., Stern, C. R., Mouradi, M. (2011). A Chemical composition of biotite as a guide to petrogenesis of granitic rocks from Maherabad, Dehnow, Gheshlagh, Khajehmourad, and Najmabad, Iran. *Iranian Journal of Crystallography and Mineralogy*, **18**, 89–100.

Kesler, S., Jones, L., Walker, R. (1975). The Intrusive rocks associated within porphyry copper mineralization on the island arc magmas. *Economic Geology*, **70**(3), 515–526. https://doi.org/10.2113/gsecongeo.70.3.515

Lalonde, A. (1993). The Composition and color of biotite from granites: mainly, two useful properties in the characterization of plutonic suites from the Hepburn internal zone of Wopmay orogen, Northwest Territories. *The Canadian Mineralogist*, **31**, 203–217.

Leng, Q. F., Tang, J. X., Zheng, W. B., Wang, B. H., Tang, P., Wang, H. (2016). A Geochronology, geochemistry and zircon Hf isotopic compositions of the ore-bearing porphyry within the Lakange porphyry Cu- Mo deposit, Tibet. *Earth Science*, **41**(6), 999– 1015.

Li, H. L., Bi, X. W., Hu, R. Z., Peng, J. T., Shuang, Y., Li, Z. L., Li, X. M., Yuan, S. D. (2007). Mineral chemistry of biotite in the Qitianling granite associated with the Furong tin deposit: Tracing tin mineralization signatures. *Acta Petrologica Sinica*, **23**(10), 2605–2614. [In Chinese with English abstract].

Li, H. L., Bi, X. W., Tu, G. C., Hu, R. Z., Peng, J. T., Wu, K. X. (2007a). The Mineral chemistry of biotite from Yanbei pluton: Implications for Sn-metallogeny. *Journal of Mineralogy and Petrology*, **27**(3), 49–54. [In Chinese with English abstract]

Liu, S. A., Li, S., He, Y., Huang, F. (2010). A Geochemical contrast between early Cretaceous ore-bearing and ore-barren high- Mg adakites in central-eastern China: Implications for petrogenesis and Cu-Au mineralization. *Geochimica et Cosmochimica Acta*, **74**(24), 7160–7178. https://doi.org/10.1016/j.gca.2010.09.003

Loferski, P. J., Ayuso, R. A. (1995). The Petrography and mineral chemistry of the composite Deboullie pluton, northern Maine, USA: Implications for the genesis of Cu-Mo mineralization. *Chemical Geology*, **123**(1-4), 89–105. https://doi.org/10.1016/0009- 2541(95)00050-V

Mengason, M. J., Candela, P. A., Piccoli, P. M. (2011). The mineral including Molybdenum, tungsten, and manganese partitioning in the system pyrrhotite–Fe–Si–O melt–rhyolite melt: Impact of sulfide segregation on arc magma evolution. *Economic Geology*, **106**(5), 855–870. https://doi.org/10.2113/econgeo.106.5.855

Munoz, J. L. (1984). F–OH and Cl–OH exchange in micas with applications to hydrothermal ore deposits. *Reviews in Mineralogy and Geochemistry*, **13**(1), 469–493.

Munoz, J. L., (1992). Calculation of the HF and HCl fugacities from a biotite composition: Revised equations. *Geological Society of America Abstracts with Programs*, **24**, A221.

Munoz, J. L., Ludington, S. D. (1974). Fluoride– hydroxyl exchange within biotite. *American Journal of Science*, **274**(4), 396–413. https://doi.org/10.2475/ajs.274.4.396

Munoz, J. L., Swenson, A. (1981). Chloride–hydroxyl exchange in the biotite and estimation of relative HCl/HF activities in magmatic-hydrothermal systems. *American Mineralogist*, 66(5–6), 477–493.

Nachit, H., Razafimahefa, N., Stussi, J. M., Carron, J. P. (1985). The Composition critiques biotites et typologie magmatiquedes granitoids. *Comptes Rendus Hebdomadaires de academia des Sciences*, **301**(11), 813–818.

Parry, W. T., Nackowski, M. P. (1963). Copper, lead, and zinc in biotites from Basin and Range quartz monzonites. *Economic Geology*, **58**(7), 1126–1144. https://doi.org/10.2113/gsecongeo.58.7.1126

Parsapoor, A., Khalili, M., Tepley, F. J., Maghami, M. (2015). Mineral chemistry and isotopic composition of the magmatic, re- equilibrated, and hydrothermal biotites from the Darreh-Zar porphyry copper deposit, Kerman, Southeast Iran. *Ore Geology Reviews*, **66**, 200–218. https://doi.org/10.1016/j.oregeorev.2014.09. 013

Patiño Douce, A. E. (1993). Titanium substitution in biotite: An empirical model with applications to thermometry, oxygen and water barometry, and implications for biotite stability. *Chemical Geology*, **108** (1–4), 132–162. https://doi.org/10.1016/0009-2541(93)90321-9

Qin, K. Z., Zhang, L. C., Ding, K. S., Xu, Y. X., Tang, D. M., Xu, X. W., Ma, T. L., Li, G. M., (2009). Mineralization types, petrogenesis of ore-bearing intrusions, and mineralogical features of the Sanchakou copper deposits in eastern Tianshan. *Acta Petrologica Sinica*, **25**(4), 845–861. (Chinese with English abstract).

Richards, J. P. (2015). The oxidation state and sulfur, Cu contents of the arc magmas: Implications for metallogeny. *Lithos*, **233**, 27–45. https://doi.org/10.1016/j.lithos.2014.12.011

Sallet, R. (2000). Fluorine as a petrogenetic tool in the quartz-bearing magmatic associations: Applications of an improved fluorine–OH biotite-apatite thermometer. *Lithos*, **50**(1–3), 241–253. https://doi.org/10.1016/S0024-4937(99)00055-6

Selby, D., Nesbitt, B. E. (2000). The Biotite chemistry from the Casino porphyry Cu–Au– Mo deposit, Yukon, Canada: Assessing magmatic and hydrothermal fluid compositions. *Chemical Geology*, **171**(1–2), 77–93. https://doi.org/10.1016/S0009-2541(00)00232-4

Shabani, A. A., Lalonde, A. E., Whalen, J. B., (2003). Composition of biotite from granitic rocks of the Canadian Appalachian orogen: A potential tectonomagmatic indicator. *The Canadian Mineralogist*, **41**(6), 1381–1396. https://doi.org/10.2113/gscanmin.41.6.1381

Sillitoe, R. H. (2015). Epithermal paleosurface of the Mineralium Deposita of Asia science **50**(7), 767–793. https://doi.org/10.1007/s00126-015-0614-z

Speer, J. A. (1981). Petrology of cordierite- and almandine-bearing granitoid plutons of the southern Appalachian Piedmont, USA. *The Canadian Mineralogist*, **19**, 35–46.

Speer, J. A. (1984). Two Mica in igneous rocks. *Reviews in Mineralogy and Geochemistry*, **13**(1), 299–356.

Tang, P., Chen, Y. C., Tang, J. X., Zheng, W. B.,Leng, Q. F., Lin, B., Fang, X. (2016).Typomorphic characteristics and geological significance of biotites in the Jiama porphyry deposit system, Tibet.

Mineral Deposits, **35**(4), 846–866. [In Chinese with English abstract].

Tang, P., Tang, J. X., Lin, B., Wang, L. Q., Zheng, W. B., Leng, Q. F., Gao, X., Zhang, Z. B., Tang, X. Q. (2019). Mineral chemistry of magmatic and hydrothermal biotites from the Bangpu porphyry Mo (Cu) deposit, Tibet. *Ore Geology Reviews*, **109**, 103012. https://doi.org/10.1016/j.oregeorev.2019.103012

Taylor, R. P. (1983). Comparison of biotite geochemistry of Bakircay, Turkey, and Los Pelambres, Chile, porphyry copper systems. *Institution of Mining and Metallurgy Transactions,* **92**, 16–22.

Tischendorf, G., Förster, H., Gottesmann, B. (2001). Minor- and trace-element composition of trioctahedral micas: A review. *Mineralogical Magazine,* **65**(2), 249–276. https://doi.org/10.1180/002646101550244

Tischendorf, G., Gottesmann, B., Förster, H. J., Trumbull, R. B. (1997). On Li-bearing micas: Estimating Li from electron microprobe analyses and an improved diagram for graphical representation. *Mineralogical Magazine,* **61**(5), 809–834. https://doi.org/10.1180/minmag.1997.061.40 9.02

Wang, L. L., Mo, X. X., Li, B., Dong, G. C., Zhao, Z. D. (2006). Geochronology and geochemistry of ore-bearing porphyry in the Qulong Cu (Mo) deposit, Tibet. *Acta Petrologica Sinica*, **22**(4), 1001–1008. (In Chinese with English abstract).

Wones, D. R., Eugster, H. P. (1965). Stability of biotite: Experiment, theory, and application. *American Mineralogist,* **50**(9), 1228–1272.

Xiong, X. L., Shi, M. Q., Chen, F. R. (2001). Biotite as a tracer of Cu and Au mineralization in hypogene-subvolcanic plutons. *Mineral Deposits*, **21**(2), 107–111. (In Chinese with English abstract).

Yang, M. Z. (1964). The alteration of hydrothermal biotite in disseminated molybdenum deposits, Eastern China. *Acta Geologica Sinica*, **44**(2), 191–212.

Yavuz, F. (2003). Evaluating micas in petrologic and metallogenic aspects: Part II—Applications using the computer program Mica+. *Computers & Geosciences,* **29**(10), 1215–1228. https://doi.org/10.1016/j.cageo.2003.08.002

Zarasvandi, A., Rezaei, M., Raith, J. G., Pourkaseb, H., Asadi, S., Saed, M., Lentz, D. R. (2018). Metal endowment reflected in the chemical composition of silicates and sulfides of the mineralized porphyry copper systems, Urumiyeh–Dokhtar magmatic arc, Iran. *Geochimica et Cosmochimica Acta*, **223**, 36–59. https://doi.org/10.1016/j.gca.2017.11.034

Zhang, W., Lentz, D. R., Thorne, K. G., McFarlane, C. (2016). A geochemical characteristic of biotite from felsic intrusive rocks around the Sisson Brook W–Mo–Cu deposit, west- central New Brunswick: As a Indicators of halogen and oxygen fugacity in magmatic systems. *Ore Geology Reviews*, **77**, 82–96. https://doi.org/10.1016/j.oregeorev.2016.02.004

Zhou, Z. X. (1986). The origin of intrusive masses in Feng Shandong, Hubei province. *Acta Petrologica Sinica,* **2**(1), 59–70. (In Chinese with English abstract).

Zhu, C., Sverjensky, D. A. (1991). Partitioning of fluorine, chlorine, and hydroxyl ions between minerals and hydrothermal fluids. *Geochimica et Cosmochimica Acta,* **55**(7), 1837–1858. https://doi.org/10.1016/0016-7037(91)90028-4

Zhu, C., Sverjensky, D. A. (1992). The Partitioning of fluorine, chlorine, and hydroxyl ions between biotite and apatite. *Geochimica et Cosmochimica Acta,* **56**(9), 3435–3467. https://doi.org/10.1016/0016-7037(92)90389-6